

# Analysis of the fluid-structure interaction of a 2D model of the savonius rotor, using immersed boundary and fourier pseudospectral methods

Mylena Carvalho Silva<sup>1</sup>, Andreia Aoyagui Nascimento<sup>1,2</sup>

<sup>1</sup>Laboratory of Thermal and Fluid Engineering (LATEF), School of Electrical, Mechanical and Computing Engineering (EMC), Federal University of Goiás (UFG)

Av. Esperança, Al. Ingá, Prédio: B5, Campus Samambaia, Goiânia 74690-900, GO, Brazil

mylenacarvalhosilva0@gmail.com, aanascimento@ufg.br

<sup>2</sup>Center of Excellence in Hydrogen and Sustainable Energy Technologies (CEHTES)

Parque Tecnológico Samambaia, Rodovia R2, n. 3.061, Campus Samambaia, CEP: 74690-900, Goiânia, Goiás, Brazil

aanascimento@ufg.br

**Abstract.** Savonius rotors are a unique type of vertical axis wind turbine (VAWT) characterized by its “S” shape, with low rotational speed, low noise and good automatic start-up capability. This turbine has a great profile for small businesses and residences. The present work presents a simplified modeling of the fluid-structure interaction problem of a Savonius rotor, using the Fourier pseudospectral method (FPSM) coupled to the immersed boundary method (IBM), considering the Newtonian fluid, incompressible flow, without heat transfer and gravitational effects, with constant and two-dimensional (2D) properties. The results presented address the flow over a freely rotating vertical turbine, which allows the analysis of the evolution of the moment coefficient ( $C_m$ ) in relation to temporal evolution, azimuthal position ( $\theta$ ) and the blade tip speed ratio ( $\lambda$ ).

**Keywords:** Savonius Rotor, Vertical Axis Turbine, Computational Fluid Dynamics (CFD), Immersed Frontier, Pseudospectral Fourier

## 1 Introduction

Wind turbines are devices that convert wind energy into electrical power. Currently, these turbines come in various models and sizes. The primary distinguishing feature among turbines is the rotor axis orientation, with two main types being widely used: Vertical Axis Wind turbines (VAWT) and Horizontal Axis Wind Turbines (HAWT).

The Savonius turbine is a VAWT model, initially developed by Savonius [1]. It is recognized for its S-shape and contains blades that operate with concave and convex side, which collect wind and convert its energy [2]. Despite its characteristic shape, the Savonius turbine can have more blades or other variations that have been developed to increase its efficiency [3] [4].

This rotor has been the subject of studies intended to: analyze the overlap rates in a freely rotating turbine [5]; the flexibility of the turbine blades [6] [7]; the positive and negative overlap with both fixed and flexible blades [8]. The simulations conducted in 3D enables the exploration of overlapping stages [9] and elliptical rotor blades [7]. Alom and Saha [10] and Tian et al. [11] indicate how the behavior of the Savonius turbine can be well represented in two-dimensional models. However, these numerical studies mostly use turbulence models, but Ueda [12] investigates the simulation of the freely rotating Savonius rotor in a transient flow with a Reynolds number  $Re_D = 500$  and different moments of inertia (MOI).

Numerical methods like finite volume method (FVM) and finite element method (FEM) are popularly used for solving such numerical simulations, however, this research aims to implement a methodology that involves the combination of the Fourier Pseudospectral Method (FPM) and the Immersed Boundary Method (IBM) for fluid-structure interaction simulations [13]. The application of these methods has yielded good results for both simulations with and without fluid-structure interaction [14] [15] [13], while also offering considerably lower computational costs for two-dimensional simulations [16].

This work simulate the flow-induced rotation of the S-shaped rotor of the Savonius model, using the Fourier pseudospectral method coupled with the immersed boundary method (IMERSPEC), considering the rotor mechanism starting automatically from a quiescent state. For a real VAWT, the influence of an external spring and

damping plays an important role in its performance. However, as a preliminary step, the present study neglects such influence.

## 2 Mathematical Model

### 2.1 Mathematical Model of Flow

The fluid dynamic behavior of the flow over the rotor is governed by the continuity equation, eq. (1), and the Navier-Stokes equation, eq. (2),

$$\frac{\partial u_i}{\partial x_i} = 0, \quad (1)$$

$$\frac{\partial u_i}{\partial t} + \frac{\partial}{\partial x_j}(u_i u_j) = -\frac{\partial p}{\partial x_i} + \nu \frac{\partial^2 u_i}{\partial x_j \partial x_j} + f_i, \quad (2)$$

where  $t$  represents time (s),  $u_i(\mathbf{x}, t)$  is the vector velocity ( $m/s$ ),  $\mathbf{x}$  is the position vector of the Eulerian field in two dimensions. The term  $p = p^*/\rho$  is calculated as a ratio between the static pressure field  $p^*$  ( $N/m^2$ ) and the fluid mass density  $\rho$  ( $kg/m^3$ ). The term  $\nu$  represents the kinematic viscosity of the fluid ( $m^2/s$ ). Lastly,  $f_i = f_i^*/\rho$  relates to the force  $f_i^*$  in ( $N/m^3$ ) and the mass density. The source term  $f_i^*$  denotes the force to which the field is subject, such as gravitational force, interfacial stresses, drag, and lift forces, among others.

The imposed force field on the flow shapes the interaction between the geometry interface and the flow field. The simulation in this study employs a two-dimensional mathematical model, incompressible, isothermal, with Newtonian fluid, and constant physical properties of both fluid and geometry.

### 2.2 Pseudospectral Fourier Method

The pseudospectral Fourier method transforms the primitive variables from physical space to spectral space using the discrete Fourier transform [17]. Thus, the eq. (1), transformed into spectral space becomes eq. (3), defining a plane of zero divergence,

$$ik_j \hat{u}_j = 0, \quad (3)$$

where  $\hat{u}(k, t)$  is the velocity field in spectral space,  $k$  is the wave vector, and  $i$  is the imaginary unit  $\sqrt{-1}$ . The linear momentum equation, eq. (2), transformed into Fourier spectral space becomes eq. (4),

$$\frac{\partial \hat{u}_i}{\partial t} + ik_j (\widehat{u_i u_j}) = -ik_i \hat{p} - \nu k^2 \hat{u}_i + \hat{f}_i, \quad (4)$$

where  $k^2$  is the square of the wave number vector  $\mathbf{k}$  and is calculated as  $k^2 = k_j k_j$ .

The advective term of eq. (4), after transformation into spectral space, results in a convolution term. Solving this term entails high computational cost; therefore, this dissertation employs the pseudospectral method presented by Canuto et al. [18] and validated in the works of Mariano [19], Nascimento et al. [15], and Nascimento et al. [20].

### 2.3 Immersed Boundary Method (IBM)

The immersed boundary method employs two independent domains: the Lagrangian domain ( $\Gamma$ ) for the immersed geometry in the fluid, and the Eulerian domain ( $\Omega$ ) for the fixed Cartesian plane representing the flow [21].

The source term can be written as,

$$f_i(\mathbf{x}, t) = \sum_{\Gamma} D_h(\mathbf{x} - \mathbf{X}) F_i(\mathbf{X}, t) \Delta s^2, \quad (5)$$

influenced by the Lagrangian force ( $F_i$ ), the spacing between the points defining the geometry ( $\Delta s$ ), and the distribution function,

$$D_h(\mathbf{x} - \mathbf{X}) = \frac{1}{\Delta x^2} W_h(r_x) W_h(r_y), \quad (6)$$

where  $r_x = \frac{x-X}{\Delta x}$ ,  $r_y = \frac{y-Y}{\Delta y}$ ,  $\Delta x$  and  $\Delta y$  are the spacings between points in the Eulerian mesh in  $x$  and  $y$ , respectively, and  $W_c$  is the weight function,

$$W_c(r) = \begin{cases} 1 - \frac{1}{2}|r| - |r|^2 + \frac{1}{2}|r|^3 & \text{if } 0 \leq |r| < 1 \\ 1 + \frac{11}{6}|r| + |r|^2 - \frac{1}{6}|r|^3 & \text{if } 1 \leq |r| < 2 \\ 0 & \text{if } 2 \leq |r| \end{cases}, \quad (7)$$

computed with respect to the previously indicated  $r$ .

More details on the combination of the Pseudospectral Fourier method and the immersed boundary method, leading to the IMERSPEC methodology, can be found in the work by Mariano et al. [13].

## 2.4 Dynamics of Rigid Body

The present analysis focuses on pure rotation about a fixed point. The material is considered continuous, with constant density ( $\rho_s$ ) throughout the geometry. Therefore, the pure rotation at fixed point  $O$  of the rotor is updated successively at each time step by eq. (8),

$$M_0 = I_0 \frac{d\Omega}{dt}, \quad (8)$$

where  $M_0$  is the resulting moment acting on the body,  $I_0$  represents the rotor moment of inertia relative to the fixed point  $O$ , and  $\frac{d\Omega}{dt}$  denotes the rate of change of angular velocity  $\Omega$  over time  $t$ .

The moment coefficient ( $C_m$ ) for the turbine can be calculated as

$$C_m = \frac{4M_0}{\rho D^2 U_\infty^2}. \quad (9)$$

and the power coefficient ( $C_p$ )

$$C_p = \frac{2M_0\Omega}{\rho D U_\infty^3} = \lambda C_m \quad (10)$$

where  $\rho$  is the fluid density,  $D$  the turbine diameter,  $U_\infty$  the free stream velocity and  $\lambda = \frac{\Omega D}{2U_\infty}$  the tip speed ratio.

## 3 Results and Discussions

At the onset of the flow, the pressure generated by the fluid's contact with the rotor surface, and the viscous force induces a rotational moment on the rotor, initiating its immediate rotational motion. The Sanovius rotor, as shown in Fig. 1, is modeled with the dimensional properties described by Ueda [12], with  $a_1 = 0.5$ ,  $a_2 = 0.35$ , and the rotor thickness at  $2a_3 = 0.15$ .

The parameters used in the simulation are: Reynolds number  $Re_D = U_\infty D / \nu = 500$ , free-stream velocity  $U_\infty = 1$  (m/s), Courant number  $CFL = 0.1$ , density ratio  $\rho_s / \rho = 13.01$ , and an initial rotor angle of  $90^\circ$  with a moment of inertia  $I_0 = 1$  ( $kg \cdot m^2$ ). The computation is carried out up to  $t^* = 2U_\infty t / D = 50$ . By the end of the simulation, the rotor completes 12 stable rotation periods. A grid of  $(N_x \times N_y) = 1024 \times 512$  collocation points is used for the Eulerian domain. The surface of the S-shaped rotor is constructed using a total of 800 lagrangian points, with the rotor tips rounded with 40 points each to prevent spurious numerical errors.

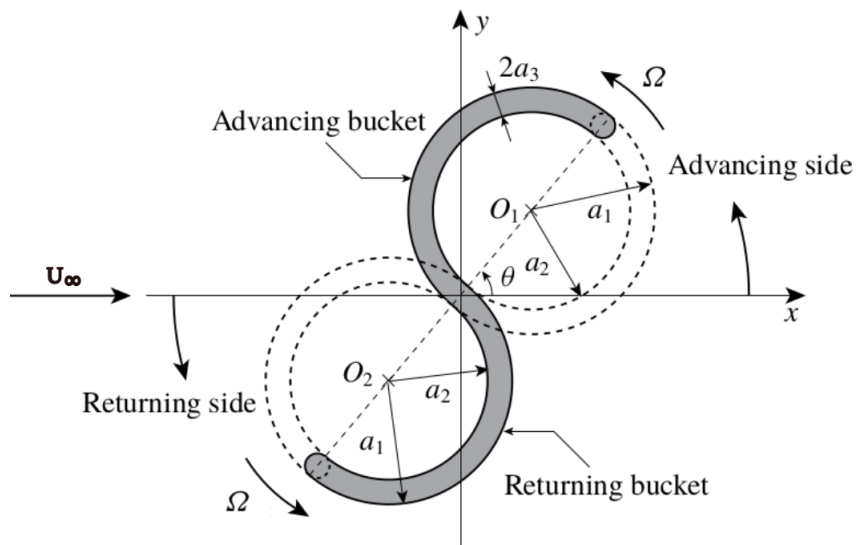


Figure 1. Notation for an Savonius rotor (Ueda [12], adapted)

The temporal evolution of the vorticity field shown in Fig. 2 indicates the behavior of the rotor during start-up. At  $t^* = 0$ , the turbine is in the initial position, with the angle  $\theta = 90^\circ$  relative to the  $x$  axis. At  $t^* = 2$ , the rotor is

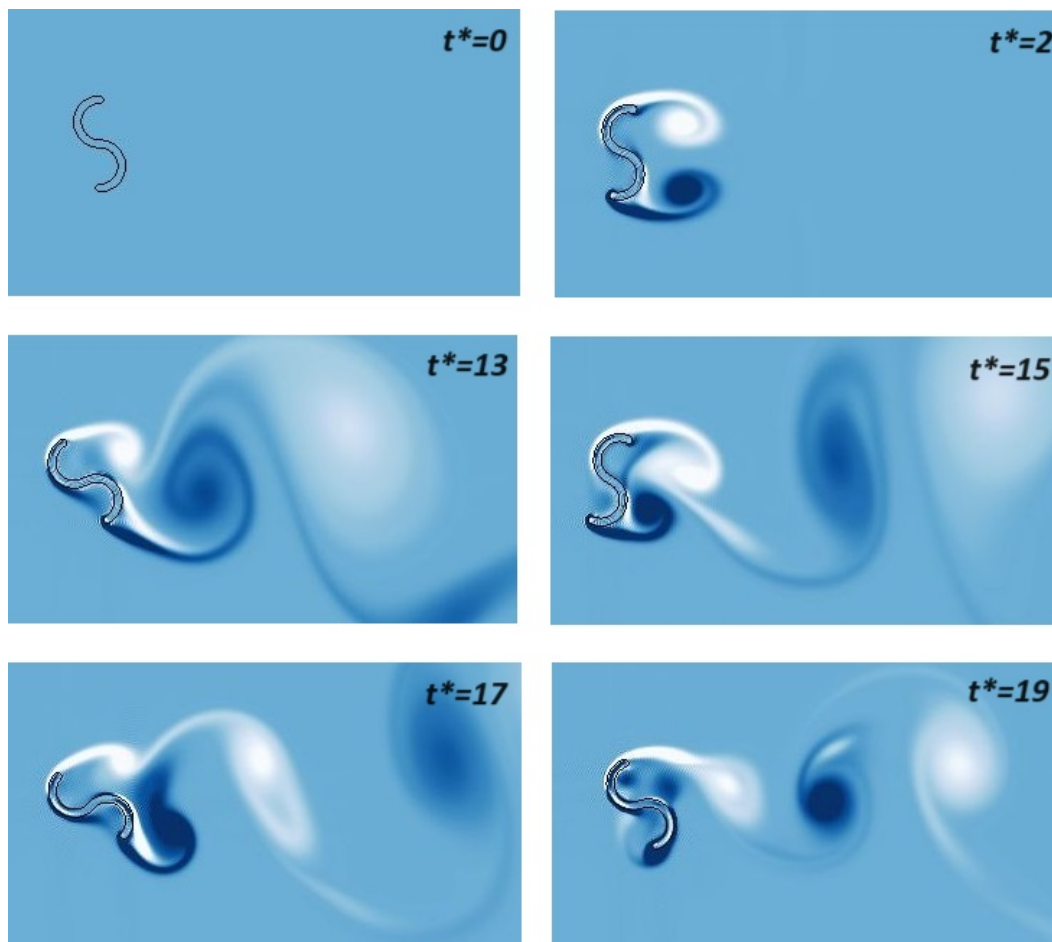


Figure 2. Temporal evolution of the vorticity field  $-5 \leq \omega_z \leq 5$ .

at  $\theta \approx 89.25^\circ$ , and the recirculations develop symmetrically with a positive direction ( $\omega_z \geq 5$ ) on the lower blade

and a negative direction ( $-5 \leq \omega_z$ ) on the upper blade. At  $t^* = 13$ , the turbine reaches  $\theta \approx 119.9^\circ$ , the wake in the vorticity field is formed, and the development of a negative recirculation downstream of the upper blade causes the rotor to rotate again in the negative (clockwise) direction. Subsequently, at  $t^* = 15$ , the rotor is at  $\theta \approx 65.22^\circ$ . Shortly afterward, the rotor returns to positive rotation (counterclockwise), reaching  $\theta \approx 186.79^\circ$  at  $t^* = 17$  and  $\theta \approx 291^\circ$  at  $t^* = 19$ . The direction of the turbine's rotation is then maintained until the end of the simulation.

The small oscillations observed in the vorticity field, near the geometry (Fig. 2), are caused by a discontinuity in the spectral domain, resulting from the imposition of the Lagrangian domain [22] [19] [14] [16] [20]. This effect becomes more evident during post-processing, as seen in the vorticity field images. It is worth noting that the IMERSPEC methodology currently employed does not use filtering, allowing spectral domain continuity interferences to manifest as oscillations in the vorticity field.

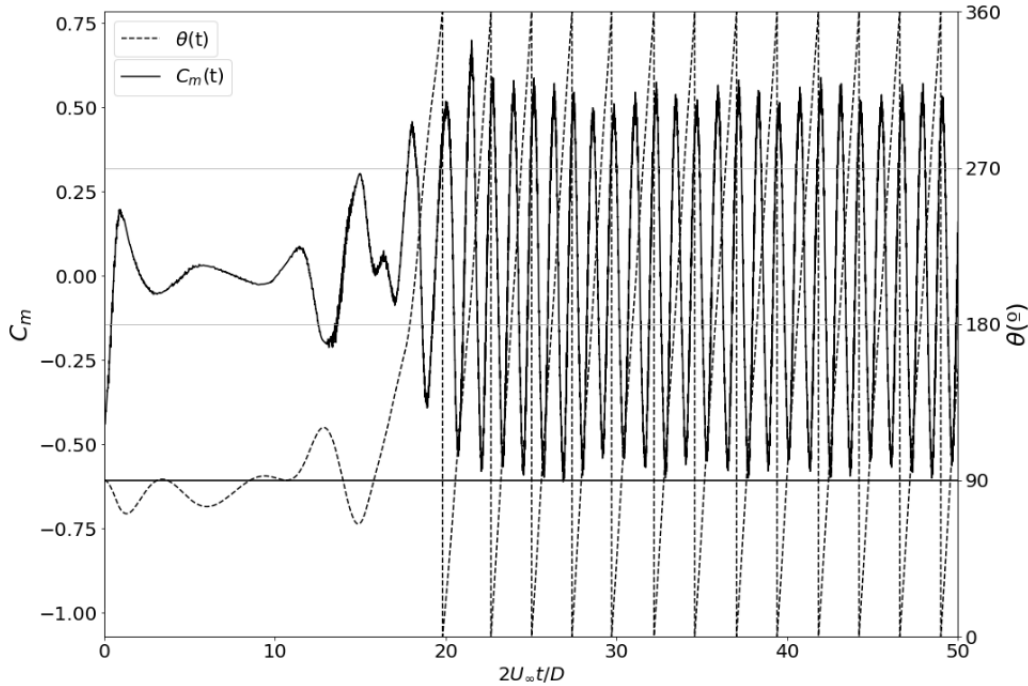


Figure 3. Time variations of  $\theta(t)$  and  $C_m$ .

Figure 3 shows the computed behavior of the rotor, indicating the angular variation  $\theta(t)$  by the dashed line and the temporal evolution of the moment coefficient  $C_m$  by the solid line. Starting with the rotor displaced by  $\theta = 90$ , the rotor initially moves in the negative (clockwise) direction, as previously discussed. The rotor then oscillates, rotating in both directions, until  $t^* \approx 15.8$ , where the rotational displacement increases until completing the first revolution at  $t^* \approx 19.82$ .

The moment coefficient ( $C_m$ ), after the second revolution of the rotor at  $t^* = 22.65$ , shows an average value of  $C_m = 0.0028$ . As demonstrated by Ueda [12], we have  $C_m \approx 0$  in a transient flow with low Reynolds number (within less than  $10^{-2}$ ).

However, during the development of the flow, the most significant deviation from the reference is observed in the angular velocity. As shown in Fig. 4, the moment coefficient behavior is demonstrated over the variation of simulation time. After reaching a steady state, the mean angular velocity of the rotor becomes  $\Omega(t) \approx 0.86$ , once it attains uniform behavior. However, in the reference data, this behavior diverges, showing  $\Omega(t) \approx 0.5$ . The tip speed ratio  $\lambda$  becomes  $\lambda \approx 0.73$ . This discrepancy is possibly due to the consideration of viscous and pressure forces. In comparison, the reference data [12] are calculated considering only the contribution of pressure.

From the moment coefficient and tip speed ratio  $\lambda$ , it is possible to obtain the power coefficient of the rotor, as indicated in (10). The power coefficient obtained for transient flow with a low Reynolds number ( $Re_D = 500$ ) is  $C_p = 0.002044 \approx 0.2\%$ . Using the same data employed to calculate the power coefficient, it is possible to identify that for the same geometric, kinematic, and dynamic parameters analyzed, but without considering the viscous force, the results presented in the literature indicate  $C_p \approx 0$  (within less than  $10^{-2}$ ) [12].

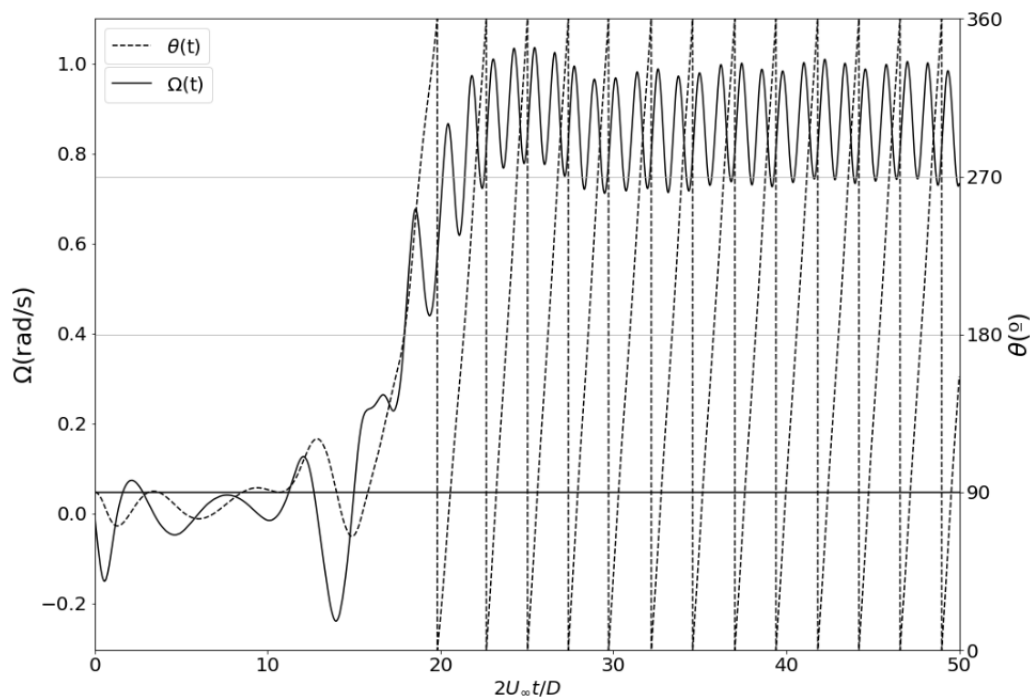


Figure 4. Time variations of  $\theta(t)$  and  $\Omega(t)$ .

## 4 Conclusions

The work presented utilizes the Fourier pseudospectral methods coupled with the immersed boundary method, which together constitute the IMERSPEC methodology, to study the fluid dynamic behavior of a simplified model of the Savonius turbine. After analyzing the results presented in this work, it was possible to understand the behavior of the rotor under free rotation.

In the behavior of the rotor subjected to free rotation, the time at which the first rotation occurs, along with the average moment coefficient  $C_m$ , are reproduced in accordance with the results presented by Ueda [12]. However, the angular velocity  $\Omega(t)$  of the rotor shows higher values than those indicated in the literature, possibly due to the inclusion of the pressure term, which is not employed in the reference article.

Despite the predominance of the pressure term in the forces interacting within the flow, it is demonstrated that the viscous force has a considerable contribution in a transient flow with a low Reynolds number ( $Re_D = 500$ ).

**Acknowledgements.** The authors express their gratitude to Eletrobras, the Research and Technological Development Program (P&D) of ANEEL, the Goiás State Research Support Foundation (FAPEG), the Center of Excellence in Hydrogen and Sustainable Energy Technologies (CEHTES) and the Graduate Program in Mechanical Engineering (PPGMEC) for the financial support and infrastructure provided for the development of this research.

**Authorship statement.** The authors hereby confirm that they are the sole liable persons responsible for the authorship of this work, and that all material that has been herein included as part of the present paper is either the property (and authorship) of the authors, or has the permission of the owners to be included here.

## References

- [1] S. J. Savonius. The s-rotor and its applications. *Mechanical engineering*, vol. 53, n. 5, pp. 333–338, 1931.
- [2] J. F. Manwell, J. G. McGowan, and A. L. Rogers. *Wind energy explained: theory, design and application*. John Wiley & Sons, 2010.
- [3] K. Sobczak, D. Obidowski, P. Reorowicz, and E. Marchewka. Numerical investigations of the savonius turbine with deformable blades. *Energies*, vol. 13, n. 14, pp. 3717, 2020.
- [4] J.-H. Lee, Y.-T. Lee, and H.-C. Lim. Effect of twist angle on the performance of savonius wind turbine. *Renewable Energy*, vol. 89, pp. 231–244, 2016.

- [5] R. Hassanzadeh and M. Mohammadnejad. Effects of inward and outward overlap ratios on the two-blade savonius type of vertical axis wind turbine performance. *International Journal of Green Energy*, vol. 16, n. 15, pp. 1485–1496, 2019.
- [6] I. Marinić-Kragić, D. Vučina, and Z. Milas. Concept of flexible vertical-axis wind turbine with numerical simulation and shape optimization. *Energy*, vol. 167, pp. 841–852, 2019.
- [7] N. Alom and U. K. Saha. Influence of blade profiles on savonius rotor performance: Numerical simulation and experimental validation. *Energy Conversion and Management*, vol. 186, pp. 267–277, 2019a.
- [8] E. Marchewka, K. Sobczak, P. Reorowicz, D. S. Obidowski, and K. Jóźwik. Application of overset mesh approach in the investigation of the savonius wind turbines with rigid and deformable blades. *Archives of Thermodynamics*, vol. 42, n. 4, 2021.
- [9] K. Mrigua, A. Toumi, M. Zemamou, B. Ouhmmou, Y. Lahlou, and M. Aggour. Cfd investigation of a new elliptical-bladed multistage savonius rotors. *International Journal of Renewable Energy Development*, vol. 9, n. 3, 2020.
- [10] N. Alom and U. K. Saha. Influence of blade profiles on savonius rotor performance: Numerical simulation and experimental validation. *Energy Conversion and Management*, vol. 186, pp. 267–277, 2019b.
- [11] W. Tian, B. Song, J. H. VanZwieten, and P. Pyakurel. Computational fluid dynamics prediction of a modified savonius wind turbine with novel blade shapes. *Energies*, vol. 8, n. 8, pp. 7915–7929, 2015.
- [12] Y. Ueda. Numerical analysis of flow-induced rotation of an s-shaped rotor. *Journal of Fluid Mechanics*, vol. 867, pp. 77–113, 2019.
- [13] F. P. Mariano, L. d. Q. Moreira, A. A. Nascimento, and A. Silveira-Neto. An improved immersed boundary method by coupling of the multi-direct forcing and fourier pseudo-spectral methods. *Journal of the Brazilian Society of Mechanical Sciences and Engineering*, vol. 44, n. 9, pp. 388, 2022.
- [14] A. Nascimento, F. Mariano, A. Silveria-Neto, and E. Padilla. A comparison of fourier pseudospectral method and finite volume method used to solve the burgers equation. *Journal of the Brazilian Society of Mechanical Sciences and Engineering*, vol. 36, pp. 737–742, 2014.
- [15] A. A. Nascimento, F. P. Mariano, E. L. M. Padilla, and A. Silveira-Neto. Comparison of the convergence rates between fourier pseudo-spectral and finite volume method using taylor-green vortex problem. *Journal of the Brazilian Society of Mechanical Sciences and Engineering*, vol. 42, pp. 1–10, 2020.
- [16] A. A. Nascimento and others. Métodos pseudoespectral de fourier e fronteira imersa aplicados a escoamentos simplificados de engenharia de perfuração, 2016.
- [17] W. L. Briggs and V. E. Henson. *The DFT: an owner's manual for the discrete Fourier transform*. SIAM, 1995.
- [18] C. Canuto, M. Y. Hussaini, A. Quarteroni, and T. A. Zang. *Spectral methods: evolution to complex geometries and applications to fluid dynamics*. Springer Science & Business Media, 2007.
- [19] F. Mariano. *Soluções Numéricas de Navier Stokes Utilizando uma hibridação das Metodologias Fronteira Imersa e Pseudospectral de Fourier*. PhD thesis, Universidade Federal de Uberlândia—Faculdade de Engenharia Mecânica, Uberlândia, 2011.
- [20] A. A. Nascimento, F. P. Mariano, da A. Silveira Neto, and E. L. M. Padilla. Coupling of the immersed boundary and fourier pseudo-spectral methods applied to solve fluid–structure interaction problems. *Journal of the Brazilian Society of Mechanical Sciences and Engineering*, vol. 46, n. 4, pp. 1–15, 2024.
- [21] F. M. White and J. Majdalani. *Viscous fluid flow*, volume 3. McGraw-Hill New York, 2006.
- [22] F. P. Mariano, L. d. Q. Moreira, A. d. Silveira-Neto, da C. B. Silva, and J. C. Pereira. A new incompressible navier-stokes solver combining fourier pseudo-spectral and immersed boundary methods. *Computer Modeling in Engineering & Sciences(CMES)*, vol. 59, n. 2, pp. 181–216, 2010.